

Photocatalytic decomposition of aqueous diazinon using reduced graphene/ZnO nanocomposite doped with manganese

Mahnaz Mohammadi^a, Afshin Maleki^{b,*}, Shiva Zandi^b, Ebrahim Mohammadi^b, Esmail Ghahremani^b, Jae-Kyu Yang^c, Seung-Mok Lee^{d,*}

^aStudent Research Committee, Kurdistan University of Medical Sciences, Sanandaj, Iran, Tel. +98-87 33661817; email: m.mohammadi7@yahoo.com

^bEnvironmental Health Research Center, Research Institute for Health Development, Kurdistan University of Medical Sciences, Sanandaj, Iran, Tel. +98-87 33661817; emails: maleki43@yahoo.com (A. Maleki), sh_rainbowz@yahoo.com (S. Zandi), emohammadi.sbums@gmail.com (E. Mohammadi), ghahremani64@gmail.com (E. Ghahremani)

^cDepartment of Environmental Engineering, Kwangwoon University, Seoul, Korea, email: jkyang@kw.ac.kr

^dDepartment of Environmental Engineering, Catholic Kwandong University, Ganeung 25601, Korea, email: leesm@cku.ac.kr

Received 1 June 2019; Accepted 22 December 2019

ABSTRACT

In this study, the photocatalytic decomposition of diazinon using graphene/ZnO nanocomposite doped with manganese was studied under UV light (UV reactor with low pressure mercury lamp 15 W) and sunlight. The effects of nanocomposite concentrations in the range of 50–200 mg/L, pH of the solution ranging from 3 to 11, diazinon concentrations in the range of 10–90 mg/L, and various contact times (20–120 min) were investigated to find the optimal conditions for diazinon decomposition. The results indicated that the photocatalytic efficiency in diazinon decomposition was 85.2% under optimal conditions (UV lamp, pH: 7, diazinon initial concentration: 10 mg/L, nanocomposite concentration: 100 mg/L, contact time: 120 min). The process efficiency under optimal conditions for the maximum removal of diazinon in the presence of sunlight was about (pH: 7, initial diazinon concentration: 10 mg/L, nanocomposite concentration: 200 mg/L and contact time: 120 min). Findings also showed that the photocatalytic process for the removal of diazinon from aqueous solutions using UV lamp radiation had a better performance than that of sunlight.

Keywords: Nanocomposite; Diazinon; Photocatalyst; Sunlight; Doping

1. Introduction

Globally, more than 800 different types of agricultural pesticides are produced. Most pesticides are categorized as persistent organic pollutants [1–3]. Adverse health effects of pesticides include short-term effects (e.g., abdominal pain, dizziness, headache, double vision, and skin problems) and long term effects (e.g., increased risk of respiratory problems, memory disorders, depression, neurological defects, cancer, and sterility) [4]. Organochlorine, organophosphate, carbamate, and pyrethroid pesticides are commonly used in

agriculture [5]. Among them, organophosphate pesticides are the largest and most diverse group of pesticides, which include about 40% of world's registered pesticides. Diazinon is one of the most widely used organophosphate pesticides [1]. Diazinon is a toxic compound with moderate risk, which is classified in category II by World Health Organization (WHO). Diazinon is slightly soluble in water (40 mg/L at 25°C), non-polar and rapidly degraded in the environment. Unlike chlorinated pesticides, it has no cumulative effect. These pesticides are resistant to degradation in the soil environment [6–8]. Therefore, entrance of these toxic compounds into groundwater resources is a growing concern.

* Corresponding authors.

Different methods have been utilized for diazinon removal from aqueous solutions such as ultrasonic waves, biodegradation, optical dispersion, ozonation, decomposition by gamma rays, Fenton process, treatment with UV/H₂O₂, adsorption and photocatalytic decomposition [9,10]. The major disadvantages in the use of these processes include complexity, low speed, high costs, high consumption of chemicals, sludge production, etc. In photocatalytic processes, pollutants are rapidly decomposed in the presence of UV or a light having ultraviolet range [11]. Photocatalytic process is based on the production of active and reactive radicals such as $\cdot\text{OH}$, and the pollutant decomposition occurs after the production of enough radicals [12–15]. Photocatalytic oxidation process in the presence of UV light and catalysts is one of the advanced oxidation processes, which can be used to remove organic contaminants [16]. This process has been taken into huge consideration due to its high efficiency, possibility of reusing catalysts repeatedly and removal of persistent pollutants [17,18]. Photocatalytic nanoparticles include titanium dioxide, zirconium dioxide, zinc oxide and graphene. Nowadays, zinc oxide is widely utilized for the oxidation of organic compounds due to the direct energy band gap, binding energy of 60 MeV, their stability against chemical corrosion, non-toxicity, insolubility, ability to break down toxic organic compounds, capability of absorbing the whole range of electromagnetic waves, and photocatalytic ability. Zinc oxide has been proposed as an important semiconductor material [19,20]. Several studies have recently reported on photocatalytic degradation of diazinon from aqueous solution [21–23]. Jonidi-Jafari et al. [24] reported removing 85% of diazinon from water using illuminated ZnO–TiO₂ composite. In another study Baneshi et al. [25] reported removal of diazinon from water using Fe–TiO₂ catalyst. They were able to achieve 98% removal efficiency.

Graphene is a layer of graphite and an allotrope of carbon with two-dimensional network structure such as honeycomb. Being one of the strongest materials, these compounds are known as the building blocks of carbon nanotubes and large fullerenes [20]. Graphene exhibits peculiar physical properties at the nano scale. Various advantages have been reported for the application of graphene such as high Young modulus (about 1,000 GPa), high resistance to breakage (130 GPa), good thermal conductivity (5,000 Wm⁻¹ K⁻¹), electrical conductivity (200,000 cm² V⁻¹ s⁻¹), specific surface area (2,600 m²g⁻¹), amazing transport phenomena such as the quantum Hall effect, adsorption of some metal ions and pollutants from soil and water [26–28]. One way to increase the photocatalytic activity of semiconductors is doping them with metals such as La, Fe, Pd, and Mn or their ions. Since the amount of energy required to initiate the photocatalytic reaction of semi-conductors such as zinc oxide and titanium dioxide is not enough in the range of visible light, doping of some metal ions on the surface of semiconductors has been widely performed to alter the band gap energy and to increase light absorption, increases photocatalytic activity. From doping with an appropriate concentration of Mn²⁺, the band gap energy of ZnO can be decreased. Several doping agents have been applied in the modification of photocatalysts [29–31].

Therefore, the main objective of this study was to synthesize and modify reduced graphene nanocomposite/ZnO

with manganese and determine its photocatalytic efficiency in diazinon removal from water solutions.

2. Experimental

2.1. Materials

Diazinon solution (60%) was prepared in Arysta Life Science, France and the rest of the required chemicals (graphite, manganese acetate, zinc acetate, sulfuric acid, and nitric acid) were purchased from Merck Co. (Germany) and used without further purification. Chemical structure and physicochemical properties of diazinon are listed in Table 1.

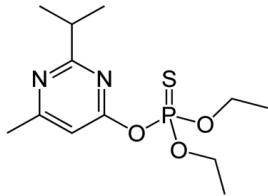
2.2. Synthesis of reduced graphene/ZnO nanocomposites doped with Mn

Graphene oxide (GO) and the reduced graphene/ZnO nanocomposites were synthesized using modified Hummers' method and solvothermal method, respectively. GO was dissolved in 80 mL of ethylene glycol (EG) by ultrasound for 2 h under ambient conditions, and subsequently was centrifuged (for 15 min at 4,000 rpm) to obtain a brown dispersion. A certain amount of manganese acetate (5 wt. %) and 80 mg of zinc acetate were dissolved in 80 mL of EG, and then, the resulted solution was added into the brown dispersion under magnetic stirring. Thereafter, 20 mg of dissolved sodium hydroxide was added in 20 mL of distilled water, and then the obtained solution was added into the mixture and was stirred for another hour to obtain a homogeneous suspension. In the next step, the suspension was held in a 200 mL Teflon autoclave stainless steel for 24 h at 160°C in order to reduce GO and achieve ZnO deposition. Finally, the prepared composite was recovered by centrifugation (for 15 min at 4,000 rpm) and washed five times with ethanol and distilled water. The synthesized nanocomposite was dried in a vacuum oven at 80°C for 24 h [31,32].

2.3. Properties of synthesized nanoparticles

X-ray diffraction (XRD), atomic force microscopy (AFM), Fourier transform infrared (FTIR) spectroscopy, scanning electron microscopy (SEM), and zeta potential analysis

Table 1
Structure and properties of diazinon

Structure	
Chemical formula	(C ₁₂ H ₂₁ N ₂ O ₃ PS)
λ_{max} (nm)	247
Molecular weight (gmol ⁻¹)	304.36
Density (20°C) (g ml ⁻¹)	1.11
WHO class	II

were used for characterizing the synthesized nanoparticles. An XRD device (Model: INEL-Equinox-3000, France) was employed to determine the crystal structures and crystal lattices of the nanoparticles. AFM (ARA Research Co, model No. 0101/A, Iran) was used to analyze the surface roughness and the surface specifications of the nanoparticles. FTIR spectrometer (Bruker, Tensor 27, Germany) was used to determine the surface functional groups of the nanoparticles. SEM (TESCAN, Czech Republic) was used for the determination of the nanoparticle shape and size. A zeta potential analyzer (Nanobrook Omni, USA) was used to measure the electric potential at the surface of the nanoparticles.

2.4. Experimental methods and analysis

The photocatalytic decomposition of diazinon was investigated using the synthesized nanocomposite as shown in Fig. 1. Diazinon solutions with different concentrations were prepared from its stock solution (1,000 ppm). After filtering the solutions, a certain amount of the synthesized nanocomposites was added to each solution and to determine the rate of diazinon decomposition under sunlight. Experiments under sunlight (with the mean lighting intensity of 1.14 mW/cm^2 , light intensity of 785 lux, and radiation angle of 67 degree) were performed in the Health Faculty, Kurdistan University of Medical Sciences, Sanandaj, in September 2015 from 10:30 AM to 12:30 PM. Thereafter, the parameters (as listed in Table 1) were analyzed. At each stage, the removal efficiency of diazinon and the effect of parameters were evaluated by changing a parameter and keeping other parameters constant. The studied parameters include nanocomposite dosage (50, 100, 150, 200 mg/L), reaction time (from 20 to 120 min), process type, initial diazinon concentration (10, 30, 50, 70, 90, 100 mg/L) and pH of the solution (3, 5, 7, 9, and 11).

To start photocatalytic experiments, a series of samples were tested under low pressure mercury lamp (15 W), which

was installed on the top of the photo reactor. In all experiments, the UV lamp was located at a distance of 15 cm from the samples. The remaining diazinon was measured using a spectrophotometer (DR5000-HACH, USA) at a wavelength of 247 nm [24].

3. Results and discussion

3.1. Nanocomposites properties

Figs. 2 and 3 show the SEM images of GO sheet and GO-ZnO-Mn.

The images of GO and GO-ZnO-Mn by SEM revealed a transparent structure for GO, which indicated that the graphene oxide was well exfoliated to single and lower layers. Fractures in the edge of the GO sheets indicated that the graphene oxide has a layered structure in all parts. Adding nanoparticles of zinc oxide and manganese to graphene oxide led to the appearance of a surface coated with beans. The spherical shaped particles with an average size between 20 and 40 nm were normally distributed on graphene and reduced graphene layers. This size is consistent with the size of the particles obtained from Scherrer formula in XRD.

The results of the FTIR in Fig. 4 showed that the peaks appeared at $3,458$; $2,923$; $1,051$; and $1,388 \text{ cm}^{-1}$, indicating stretching vibration of OH, C–H, C–O, and carbonyl groups, respectively. Another peak appeared at $1,627 \text{ cm}^{-1}$, indicating the stretching vibration of C=C groups. Peaks observed at 532 , 543 , and 450 cm^{-1} are associated with the presence of ZnO groups in the compounds. Given that in the solvothermal process, at first the graphene oxide is reduced, and then the nanocomposite is synthesized, the peak that appeared at $3,467 \text{ cm}^{-1}$ is attributed to the presence of zinc groups on the graphene oxide structure. The peak observed at 439 cm^{-1} indicated the presence of Mn in the compounds.

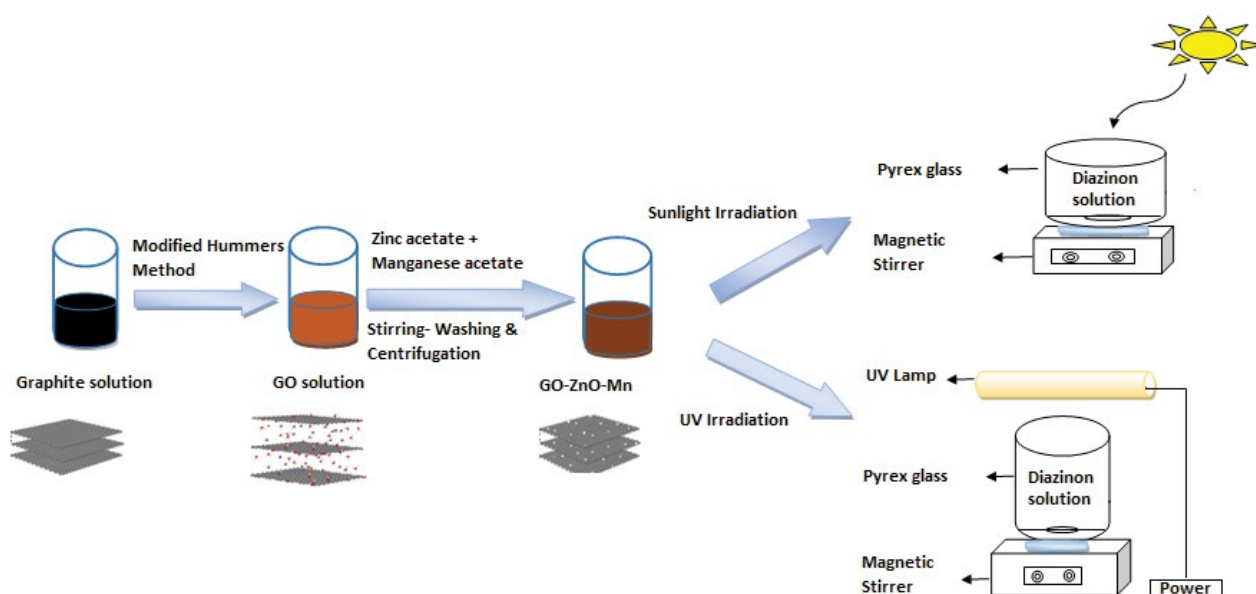


Fig. 1. Schematic of photocatalytic degradation process under sunlight and ultraviolet irradiation.

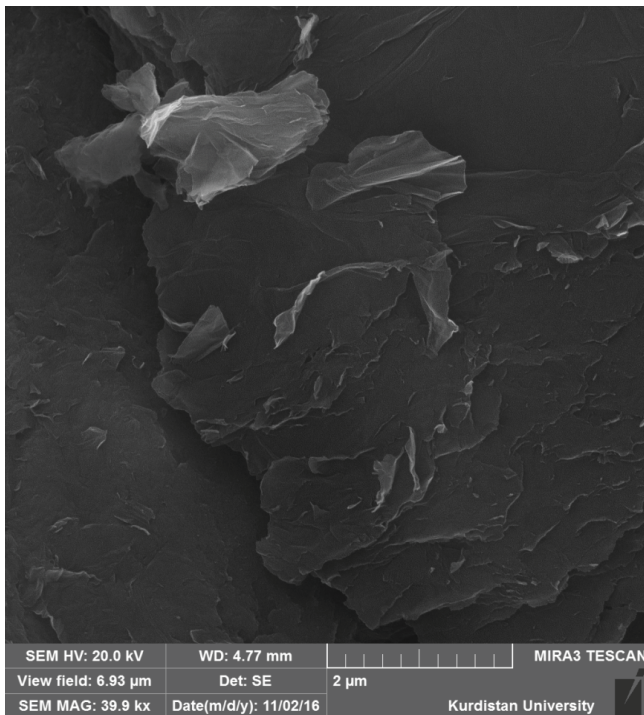


Fig. 2. SEM image of graphene oxide.

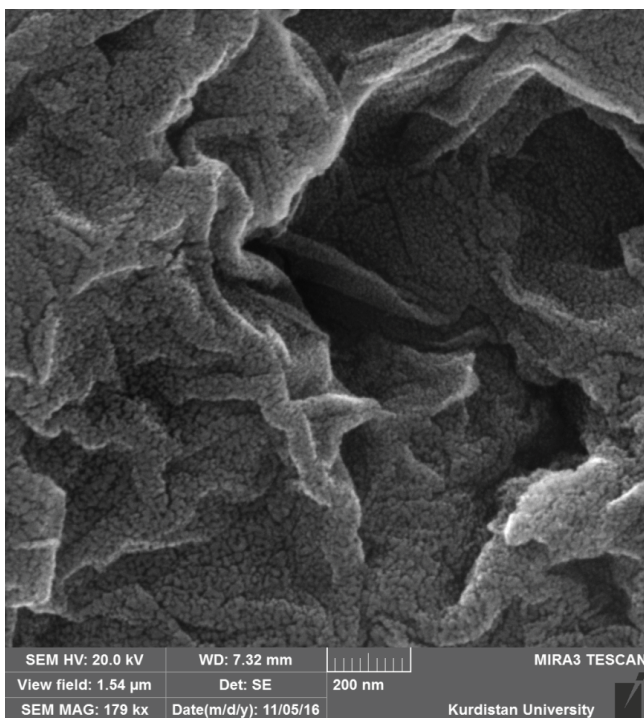


Fig. 3. SEM image of GO-ZnO-Mn nanocomposite.

In XRD pattern of graphene oxide as shown in Fig. 5, a peak with a high intensity (001) was observed at an angle of $2\theta = 11^\circ$, which indicated expansion among the layers of graphene oxide due to the oxidation of graphite and formed groups such as carboxyl, hydroxyl, and epoxy. This peak was

reduced after the synthesis of graphene oxide nanocomposites due to the formation of reduced graphene oxide. Moreover, the peaks with high intensity at (100) (002) (101) (110) (200) (112) (201), and (202) showed a high purity and hexagonal wurtzite structure on the surface of zinc oxide. With the addition of manganese, the peak of XRD was reduced to a very small and wide peak. This result revealed that the Mn-ZnO nanoparticles are well packed on the graphene oxide sheets. According to Scherrer formula (Eq. (1)), the nanoparticles' size was about 35 nm.

$$D = \frac{(K \times \lambda)}{(\beta \cos \theta)} \quad (1)$$

where K is a dimensionless shape factor, with a value close to unity. The shape factor has a typical value of about 0.9 but varies with the actual shape of the crystallite.

And D is the crystallite size (nm), β is the peak width at half maximum intensity (radians), θ is the Bragg angle of the peak (degrees) and λ is the wavelength of X-rays (nm).

The parameters of nanocomposite network are listed in Table 2.

The two and three-dimensional AFM image of graphene/ZnO in contact mode with a scanning distance of $3 \times 3 \mu\text{m}$ is shown in Fig. 6. The results of the analysis of the sizes and roughness coefficients of the nanoparticles are also shown in Fig. 6. According to AFM analysis, the diameter of the nanoparticles was 37 nm (which is consistent with XRD result) and the size between graphene oxide layers is 3–5 nm. Fig. 6a also shows the graphene oxide alone layers. As the red arrows indicate, the three distinct graphene oxide layers are well detectable. In fact, its shape is few-layered sheet with a mean thickness of 1.48 nm. Fig. 6b clearly shows the graphene oxide layers and coated nanoparticles (green arrows show the position of nanoparticles on a graphene oxide layer based on a two-dimensional AFM image). The deposition of nanoparticles on graphene oxide is well seen in the three-dimensional AMF image (Fig. 6c).

One of the most important parameters for describing the colloidal dispersion stability is the zeta potential. This measurement is related to the determination of the negative charge around the double layer related to the colloidal particle as a result of the ionization of different functional groups. It has been found that if the zeta potential is between -30 to $+30$ mV, the particles are stable due to the distribution [33]. Regarding the graphene oxide, the surface charge may depend on the amount and type of functional groups on the surface of the graphite oxide. During the synthesis of graphene oxide, functional groups such as epoxy, hydroxyl, and carboxylic groups are located on the graphene oxide sheets. The hydroxyl and carboxylic groups of the graphene oxide sheets can weakly develop negative charges in the solution [34]. Therefore, the negative charges of the GO and GO-ZnO-Mn were evaluated by zeta potential measurements at the natural pH of the dispersions at 25°C and the results are presented in Table 3 and Fig. 7. As reported in Table 3, the surface charge of the GO and GO-ZnO-Mn is -4.75 and -6.02 mV, respectively, with an increase in the surface charge of the GO after the modification which may be due to a reduction in the agglomeration of the sheets and the presence of more carboxylic groups on the surface and finally increase of colloidal stability.

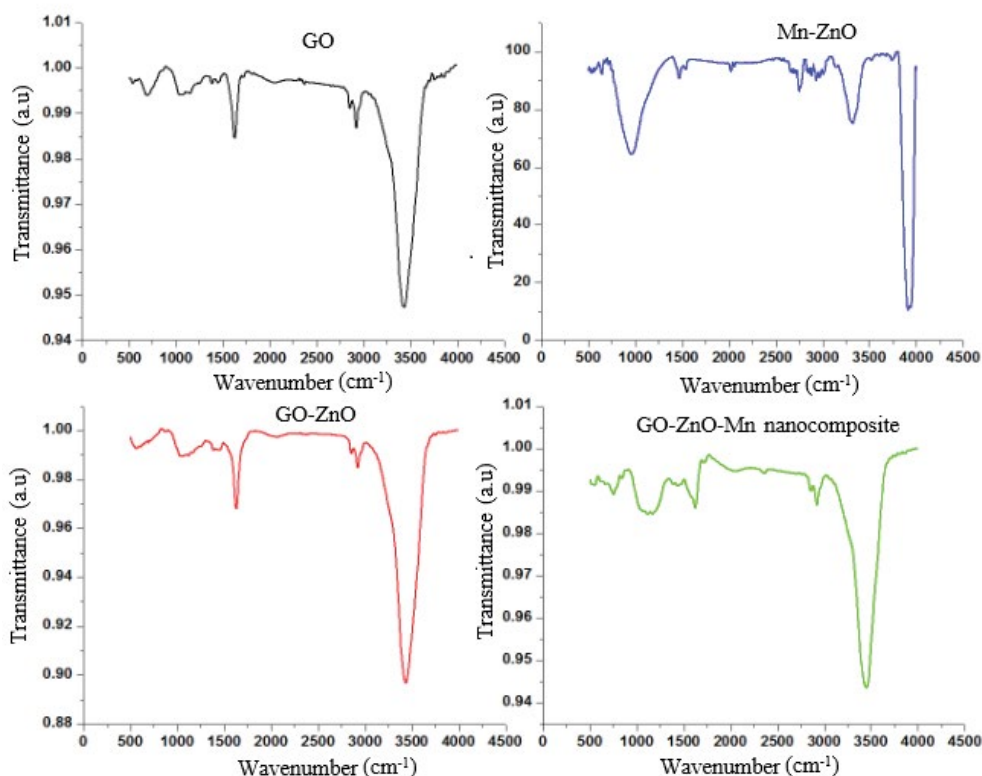


Fig. 4. FTIR spectra of GO, Mn-ZnO, GO-ZnO, and GO-ZnO-Mn nanocomposite.

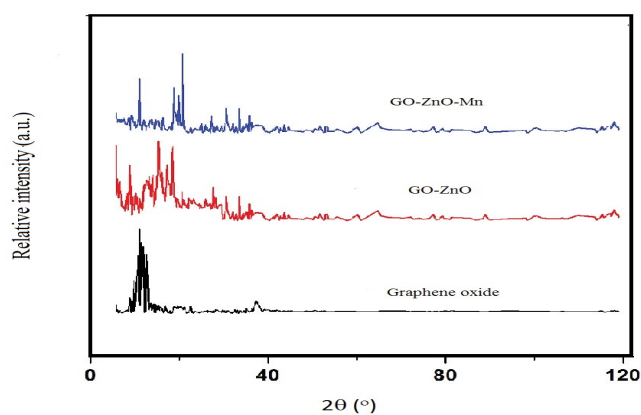


Fig. 5. XRD patterns of GO, GO-ZnO, and GO-ZnO-Mn nanocomposite.

Fig. 8 shows the dynamic light scattering (DLS) result of GO sheet and GO-ZnO-Mn with a slight difference between them. For the graphene oxide sample, the size distribution varied in the range of 34 to 1,300 nm with an average size of 217 nm (Fig. 8a). This means that these dispersions had a very broad size distribution and may contain large particles or agglomerates, suggesting that DLS analysis is not suitable for determining size. However, these sizes were reduced after modification of graphene oxide and reached about 156 nm (average size) at a range of 23–1,000 nm (Fig. 8b) which, as already mentioned, can be related to a reduction in

the agglomeration of the sheets. In general, it is important to note that the DLS analysis assumes that particles are spherical shaped. For graphene oxide which possess extremely large ratios of length or breadth to a few nanometers thickness, these results seem logical and help to determine and compare the relative change in the platelet size as a function of surface modification.

3.2. Effect of operational parameters on photocatalytic decomposition of diazinon

3.2.1. Effect of photocatalyst dosage under UV light and sunlight

Figs. 9 and 10 demonstrate the effect of nanocomposite dosage (50, 100, 150, and 200 mg/L) on photocatalytic decomposition of diazinon under UV lamp and sunlight radiation at constant diazinon concentrations of 50 mg/L and at pH 5. The results showed that the photocatalytic degradation of diazinon in the absence of GO-ZnO-Mn catalyst was negligible, and the process efficiency increased with increase in the photocatalyst dosage. The maximum removal efficiency under UV light was 55% at 100 mg/L of the photocatalyst, while it was 21% under sunlight at 200 mg/L of photocatalyst.

Also this phenomenon may be attributed to the availability of active sites and penetration of light into the suspension. In the beginning of the process, a large number of holes are formed on the surface of the photocatalyst and this leads to an increase in the system efficiency. But, at higher concentrations than 100 mg/L, increased turbidity and the

Table 2
Parameters of nanocomposite network

Sample	Nanoparticles' size (nm)	a (Å)	c (Å)	c/a ratio	Volume (Å ³)
Go-ZnO	35.2	3.249	5.2070	1.6026	27.4825
Go-ZnO-Mn	35	5.84	5.84	1	99.5883

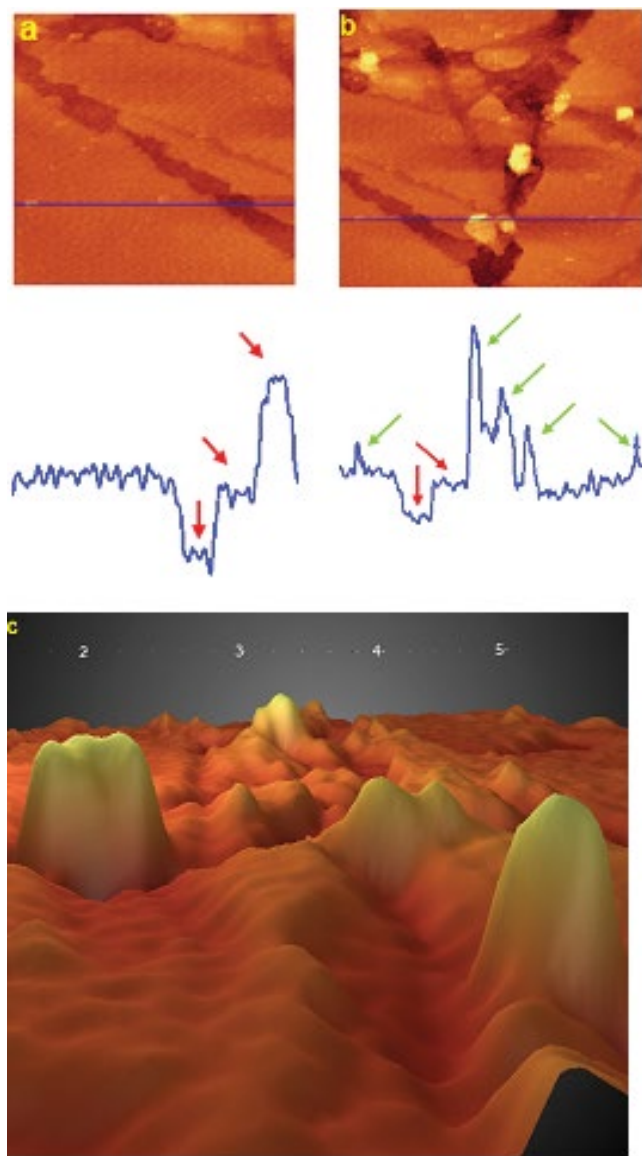


Fig. 6. AFM images of (a) GO and (b and c) GO-ZnO-Mn nanocomposite.

scattering effect of nanoparticles causes hindering light penetration and reduced removal efficiency of diazinon [35–37]. Therefore, in the presence of UV lamp, 100 mg/L of nanocomposite was selected as the optimal concentration for the next steps of experiments, and in the presence of sunlight, 200 mg/L of the nanocomposite was chosen as the optimal concentration. Meanwhile, higher intensity of UV-C (used in the UV reactor) makes it better option than sunlight for two

Table 3
Zeta potential of nanoparticle

Nanoparticles	Zeta potential (mV)	Zeta potential model	Mobility (μ/s)/(V/cm)
Go	-4.75	Hückel	-0.25
Go-ZnO-Mn	-6.02	Hückel	-0.31

reasons. First, it can produce higher numbers of electron/hole pairs and $\cdot\text{OH}$ radicals, which introduce higher active sites on the nanocomposite to remove diazinon. Second, higher numbers of $\cdot\text{OH}$ radicals and peroxides, produced by UV-C, give decomposition of diazinon even after full occupation of active sites on the nanocomposite, achieving higher removal efficiency. But, lower UV intensity of sunlight produces lower electron/hole pairs and $\cdot\text{OH}$ radical. Therefore, in a specific period of time, most of active sites on the nanocomposite get occupied and there would be lower sites for the removal of remaining diazinon and the produced analytes from its decomposition, which leads to decrease in the diazinon removal.

3.2.2. pH effect

Figs. 11 and 12 show the removal efficiency of diazinon at various pH values (3, 5, 7, 9, and 11) at constant concentration of diazinon (50 mg/L) and nanocomposite in the presence of UV lamp (100 mg/L) and sunlight (200 mg/L), respectively. Results revealed that under both UV lamp and sunlight, the process efficiency of diazinon removal increased with increase in pH from 3 to 7. The highest percentage of photocatalytic degradation of diazinon in neutral pH was 72.7% under UV lamp, and it was about 30% under sunlight. Generally, the effect of pH depends on the type of pollutants and point of zero charge (pzc) of the photocatalyst [38–41]. In this study, pH_{pzc} of the GO-ZnO-Mn nanocomposite was 7.3. According to previous studies, pK_a of diazinon is 2.6 [30], and it has a negative surface charge in pHs above this value. While the GO-ZnO-Mn nanocomposite has positive surface charge at pH values lower than 7.3. Therefore, in the pH range of diazinon pK_a and pH_{pzc} , the charge of the nanocomposite is positive and diazinon is negative, which make them attracted towards each other. At higher pH values, the negative charge causes the repulsion between diazinon and nanocomposite and reduces the photocatalytic efficiency in diazinon removal [37].

3.2.3. Effect of initial pollutant concentration

The effect of initial diazinon concentrations in photocatalytic decomposition is one of the most important parameters.

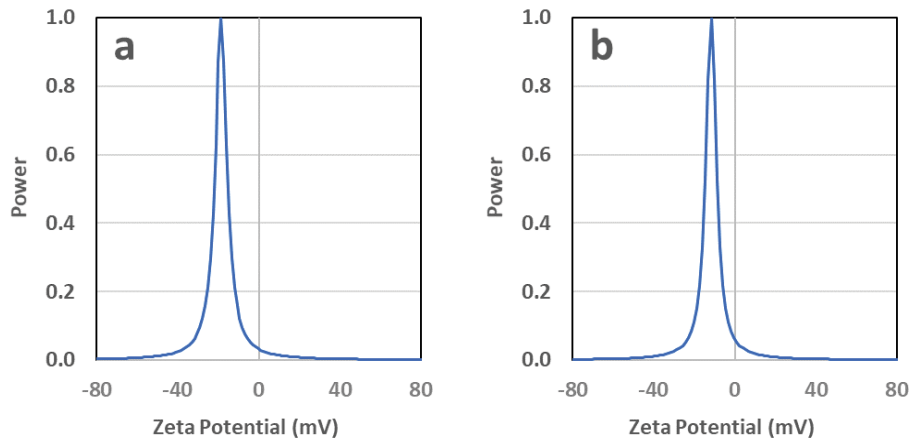


Fig. 7. Zeta potential of (a) GO and (b) GO-ZnO-Mn nanocomposite.

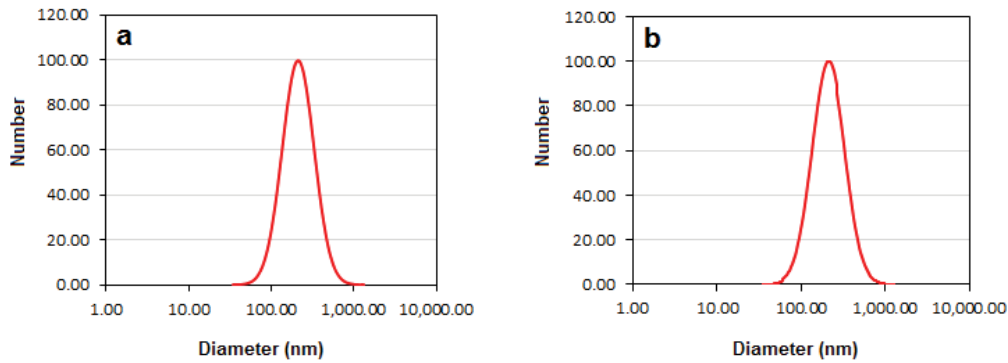


Fig. 8. Particle size distributions of (a) GO and (b) GO-ZnO-Mn nanocomposite.

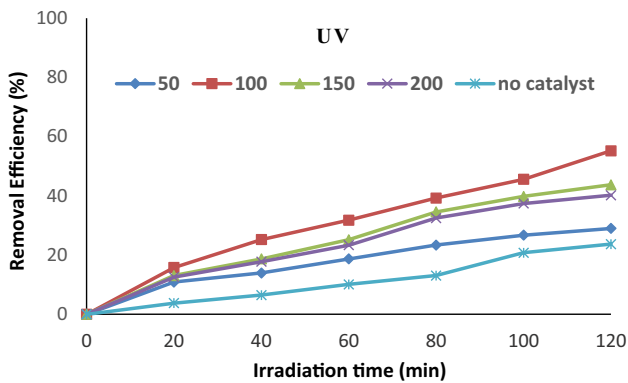


Fig. 9. Effect of photocatalyst dosage on photocatalytic decomposition of diazinon under UV irradiation (pH: 5, diazinon concentration: 50 mg/L).

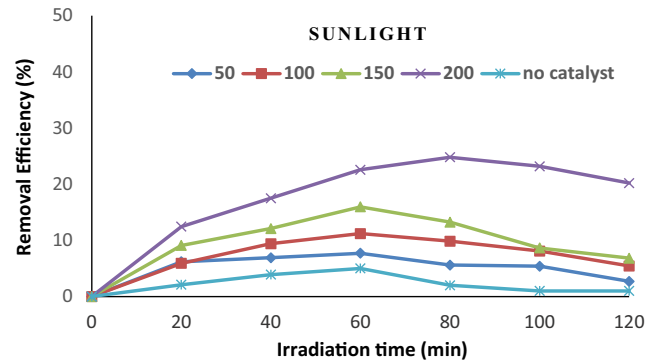


Fig. 10. Effect of photocatalyst dosage on photocatalytic decomposition of diazinon under sunlight (pH: 5, diazinon concentration: 50 mg/L).

The effect of this parameter on photocatalytic degradation of diazinon was studied at different concentrations (10, 30, 50, 70, and 90 mg/L) at pH 7 and 100 mg/L of GO-ZnO-Mn nanocomposite under UV lamp radiation, and 200 mg/L of GO-ZnO-Mn under sunlight. Fig. 13 shows the effect of UV lamp on process efficiency. According to the results, the

process efficiency decreased from 85.2% to 34% with increase in the diazinon concentration from 10 to 90 mg/L. The results of sunlight effect revealed that the removal efficiency of diazinon increased up to 35% with decreasing the diazinon concentration (Fig. 14). This trend may be due to the increased ratio of photocatalyst/diazinon which leads to higher adsorption percentages of diazinon on the photocatalyst surface at

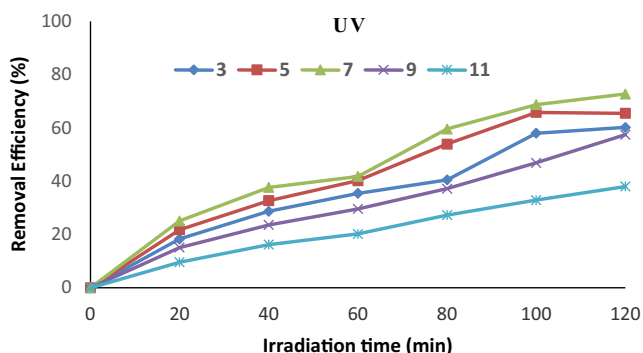


Fig. 11. Effect of initial pH on the photocatalytic decomposition of diazinon under UV irradiation (GO-ZnO-Mn nanocomposite: 100 mg/L, diazinon concentration: 50 mg/L).

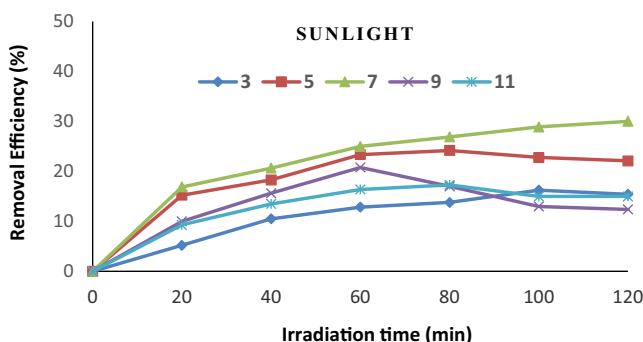


Fig. 12. Effect of initial pH on the photocatalytic decomposition of diazinon under sunlight (GO-ZnO-Mn nanocomposite: 200 mg/L, diazinon concentration: 50 mg/L).

lower concentration. Moreover, increased diazinon concentration prevents the photons from reaching the catalyst surface and consequently, the photocatalytic degradation rate is decreased. This finding is consistent with previous studies [42–44].

3.2.4. Comparing the processes

In order to survey the effect of different processes on diazinon decomposition, the removal efficiencies of diazinon by single nanoparticles, UV, and the nanoparticles in combination with UV were compared. The experimental conditions were kept constant in all studied processes (pH: 7, initial diazinon concentration: 100 mg/L and contact time: 120 min). The removal efficiency of diazinon by GO, GO-ZnO, GO-ZnO-Mn, UV, GO/UV, and GO-ZnO/UV, GO-ZnO-Mn/UV was 25%, 30%, 45%, 28%, 36%, 57%, and 85%, respectively (Fig. 15).

The photocatalytic degradation of organic materials occurs with the semiconductor optical stimulation, followed by the formation of pairs of electrons-hole on the surface of the catalyst (Eq. (2)). High oxidation potential of holes (h_{VB}^+) in the catalyst provides the direct oxidation of organic substances (pesticides) according to Eq. (3). In addition, by water splitting (Eq. (4)) or in the reaction of holes with OH^- (Eq. (5)), highly reactive $\cdot OH$ radicals are produced.

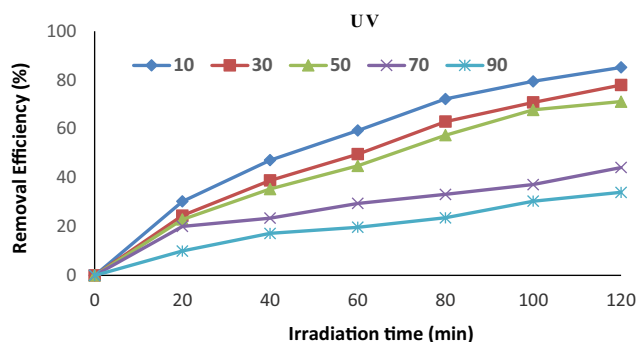


Fig. 13. Effect of initial diazinon concentration on photocatalytic decomposition of diazinon under UV radiation (pH: 7, GO-ZnO-Mn nanocomposite concentration: 100 mg/L).

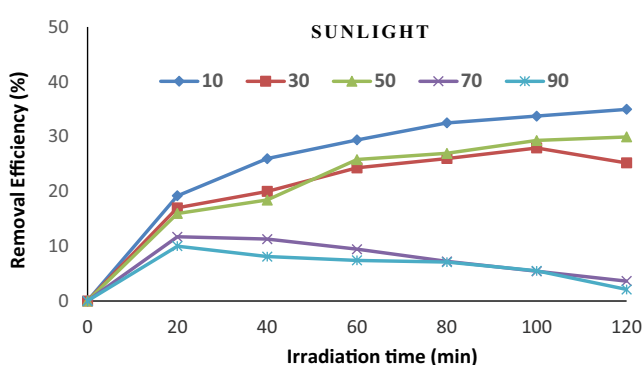


Fig. 14. Effect of initial diazinon concentration on photocatalytic decomposition of diazinon under sunlight (pH: 7, GO-ZnO-Mn nanocomposite concentration: 200 mg/L).

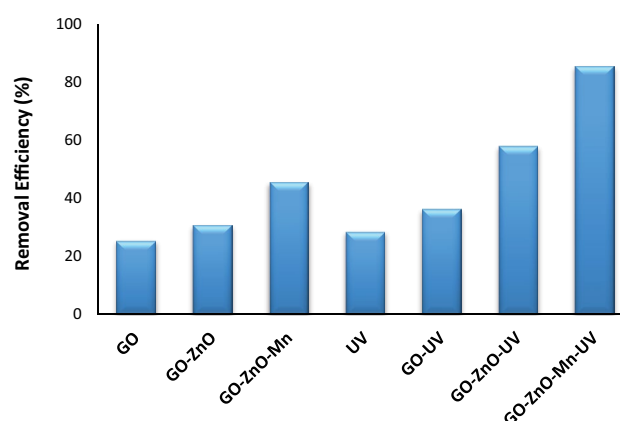
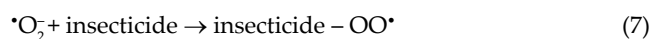
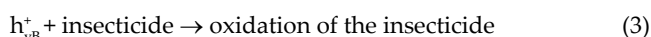


Fig. 15. Comparing the processes in photocatalytic decomposition of diazinon (pH: 7, GO-ZnO-Mn nanocomposite: 100 mg/L, initial diazinon concentration: 10 mg/L).

Electrons in conduction band on the surface of the catalyst convert the molecular oxygen to superoxide anion (Eq. (6)). In the presence of organic materials, the radicals have the ability of forming organic peroxides (Eq. (7)) or hydrogen peroxide (Eq. (8)).

Table 4
Comparison of photocatalytic degradation of diazinon

Photocatalyst	Dosage	Light source	Time (min)	Concentration (mg/L)	pH	Removal (%)	Reference
GO-ZnO-Mn	0.1 g/L	UV light (15-W low pressure UV lamp)	120	10	7	85	This study
Illuminated ZnO-TiO ₂ composite	0.5 g/L	UV light	120	20	7	85	[24]
Fe-TiO ₂ /Bent-Fe	0.5 g/L	Visible light (36 W compact bulb)	-	25	5.6	58.3	[23]
WO ₃	0.5 g/L	UV light (125- W medium-pressure UVC lamp)	120	20	3	99.88	[21]
Iron doped TiO ₂	0.4 g/L	UV light (15-W low pressure UV lamp)	100	30	5.5	76	[22]
FeFNS-doped TiO ₂	0.25 g/L	UV-LEDs	100	1.3	7	44.8	[47]
Fe ₃ O ₄ /HAP	4 g/L	UV light (30 W low-pressure lamp)	60	10	5.5	75	[48]



Moreover, the electrons in the conduction band are responsible for the production of $^{\bullet}\text{OH}$ radicals, which are shown in (Eq. (9)) as the main cause of mineralization of organic substances. In this regard, similar results have been reported by other researchers [45,46].

In order to evaluate the effect of different processes on the photocatalytic degradation of diazinon using different photocatalysts, the results of this study were compared with other reported data and summarized in Table 4. This comparison shows that the GO-ZnO-Mn is an effective photocatalyst for the degradation of diazinon compared with other photocatalysts [47,48].

4. Conclusion

In this research, nanocomposite of graphene oxide-zinc oxide doped with manganese was used for photocatalytic decomposition of diazinon from aqueous solutions. The characteristics of GO-ZnO-Mn composite were determined using SEM, AFM, XRD, and FTIR. The results revealed that GO-ZnO-Mn/UV had the maximum efficiency in diazinon removal in comparison with other processes. The

highest removal efficiency of diazinon was obtained under UV light, at neutral pH, diazinon concentration of 10 mg/L and nanoparticle concentration of 100 mg/L. And, under sunlight, it was obtained at neutral pH, diazinon concentration of 10 mg/L and nanoparticle concentration of 200 mg/L.

Acknowledgments

This research was extracted from the Master Dissertation work of the first author (IR.MUK.REC.1394.14538). The authors acknowledge the support of this work by Kurdistan University of Medical Sciences, Sanandaj, Iran. This research was also supported by Basic Science Research Program through the National Research Foundation of Korea (NRF) funded by the Ministry of Education (NRF-2019R1I1A3A01062424).

References

- [1] M. Khodadadi, M. Samadi, A. Rahmani, Comparison between the efficiency of advanced oxidation process and coagulation for removal organophosphorus and carbamate pesticides, Iran. J. Health Environ., 4 (2011) 277–288.
- [2] H. El Bakouri, J. Morillo, J. Usero, A. Ouassini, Potential use of organic waste substances as an ecological technique to reduce pesticide ground water contamination, J. Hydrol., 353 (2008) 335–342.
- [3] M. Khodadadi, M. Samadi, A. Rahmani, R. Maleki, A. Allahresani, R. Shahidi, Determination of organophosphorous and carbamate pesticides residue in drinking water resources of Hamadan in 2007, Iran. J. Health Environ., 2 (2010) 250–257.
- [4] M.C. Alavanja, J.A. Hoppin, F. Kamel, Health effects of chronic pesticide exposure: cancer and neurotoxicity 3, Annu. Rev. Public Health, 25 (2004) 155–197.
- [5] L. Kazemizad, Y. Ghaffari, M. Kermani, M. Farzadkia, A. Hajzadeh, Investigation of photo-Fenton-like process efficiency in diazinon pesticide removal from aqueous solutions, J. Saf. Environ. Health Res., 1 (2016) 17–22.
- [6] H. Shemer, K.G. Linden, Degradation and by-product formation of diazinon in water during UV and UV/H₂O₂ treatment, J. Hazard. Mater., 136 (2006) 553–559.
- [7] P. Li, E. Swanson, F. Gobas, Diazinon and its degradation products in agricultural water courses in British Columbia, Canada, Bull. Environ. Contam. Toxicol., 69 (2002) 59–65.

- [8] M. Bavcon, P. Trebše, L. Zupančič-Kralj, Investigations of the determination and transformations of diazinon and malathion under environmental conditions using gas chromatography coupled with a flame ionisation detector, *Chemosphere*, 50 (2003) 595–601.
- [9] A. Hassani, A. Khataee, S. Karaca, M.J.E.t. Shirzad-Siboni, Surfactant-modified montmorillonite as a nanosized adsorbent for removal of an insecticide: kinetic and isotherm studies, *Environ. Technol.*, 36 (2015) 3125–3135.
- [10] M. Shirzad-Siboni, A. Khataee, A. Hassani, S.J.C.R.C. Karaca, Preparation, characterization and application of a CTAB-modified nanoclay for the adsorption of an herbicide from aqueous solutions: kinetic and equilibrium studies, *C. R. Chim.*, 18 (2015) 204–214.
- [11] M.H. Fulton, P.B. Key, Acetylcholinesterase inhibition in estuarine fish and invertebrates as an indicator of organophosphorus insecticide exposure and effects, *Environ. Toxicol. Chem.*, 20 (2001) 37–45.
- [12] S. Alijani, M. Vaez, A. Zaringhalam Moghadam, Comparative study on the photodegradation of Acid Black 26 from synthetic wastewater using slurry and immobilized TiO₂ on the sackcloth fiber, *Iran. J. Health Environ.*, 6 (2013) 243–256.
- [13] S. Hemmati Borji, S. Nasser, R. Nabizadeh Nodehi, A. Mahvi, A. Javadi, Photocatalytic degradation of phenol in aqueous solutions by Fe (III)-doped TiO₂/UV process, *Iran. J. Health Environ.*, 3 (2011) 369–380.
- [14] A.H. Mahvi, A. Maleki, Photosonochemical degradation of phenol in water, *Desal. Wat. Treat.*, 20 (2010) 197–202.
- [15] A. Maleki, B. Shahmoradi, Solar degradation of Direct Blue 71 using surface modified iron doped ZnO hybrid nanomaterials, *Water Sci. Technol.*, 65 (2012) 1923–1928.
- [16] A. Maleki, A. Mahvi, M. Alimohamadi, A. Ghasri, Advanced oxidation of phenol by ultraviolet irradiation in aqueous system, *Pak. J. Biol. Sci.*, 9 (2006) 2338–2341.
- [17] M.Z. NOORI, R. Darvishi, K.A.G. SHAMS, H. Ghodini, M. Foroughi, Study of the effective parameters on decolorization of methylene blue using UV radiation in the presence of immobilized catalyst, *J. Ilam Univ. Med. Sci.*, 21 (2013) 36–46.
- [18] B. Shahmoradi, A. Maleki, K. Byrappa, Removal of Disperse Orange 25 using in situ surface-modified iron-doped TiO₂ nanoparticles, *Desal. Wat. Treat.*, 53 (2015) 3615–3622.
- [19] C. Ren, B. Yang, M. Wu, J. Xu, Z. Fu, T. Guo, Y. Zhao, C. Zhu, Synthesis of Ag/ZnO nanorods array with enhanced photocatalytic performance, *J. Hazard. Mater.*, 182 (2010) 123–129.
- [20] B. Shahmoradi, A. Maleki, K. Byrappa, Photocatalytic degradation of Amaranth and Brilliant Blue FCF dyes using in situ modified tungsten doped TiO₂ hybrid nanoparticles, *Catal. Sci. Technol.*, 1 (2011) 1216–1223.
- [21] A. Mohagheghian, K. Ayagh, K. Godini, M. Shirzad-Siboni, Using amino-functionalized Fe₃O₄-WO₃ nanoparticles for diazinon removal from synthetic and real water samples in presence of UV irradiation, *J. Adv. Oxid. Technol.*, 20 (2017) 20160153.
- [22] S. Tabasideh, A. Maleki, B. Shahmoradi, E. Ghahremani, G. McKay, Sonophotocatalytic degradation of diazinon in aqueous solution using iron-doped TiO₂ nanoparticles, *Sep. Purif. Technol.*, 189 (2017) 186–192.
- [23] N.M. Phuong, N.C. Chu, D. Van Thuan, M.N. Ha, N.T. Hanh, H.D.T. Viet, M. Thu, N. Thi, P. Van Quan, T. Truc, Novel removal of diazinon pesticide by adsorption and photocatalytic degradation of visible light-driven Fe-TiO₂/Bent-Fe photocatalyst, *J. Chem.*, 2019 (2019) 2678927.
- [24] A. Jonidi-Jafari, M. Shirzad-Siboni, J.-K. Yang, M. Naimi-Joubani, M. Farrokhi, Photocatalytic degradation of diazinon with illuminated ZnO-TiO₂ composite, *J. Taiwan Inst. Chem. Eng.*, 50 (2015) 100–107.
- [25] M.M. Baneshi, S. Rezaei, A. Sadat, A. Mousavizadeh, M. Barafraشتهpour, H. Hekmatmanesh, Investigation of photocatalytic degradation of diazinon using titanium dioxide (TiO₂) nanoparticles doped with iron in the presence of ultraviolet rays from the aqueous solution, *Biosci. Biotechnol. Res. Commun.*, 1 (2017) 60–67.
- [26] Y.H. Siddique, W. Khan, S. Khanam, S. Jyoti, F. Naz, B.R. Singh, A.H. Naqvi, Toxic potential of synthesized graphene zinc oxide nanocomposite in the third instar larvae of transgenic *Drosophila melanogaster* (hsp70-lacZ) Bg9, *BioMed Res. Int.*, 2014 (2014) 1–10.
- [27] L. Meijiao, J. Li, X. Yang, C. Zhang, J. Yang, H. Hu, X. Wang, Applications of graphene-based materials in environmental protection and detection, *Chinese Sci. Bull.*, 58 (2013) 2698–2710.
- [28] B. Saravanakumar, R. Mohan, S.-J. Kim, Facile synthesis of graphene/ZnO nanocomposites by low temperature hydrothermal method, *Mater. Res. Bull.*, 48 (2013) 878–883.
- [29] Z. Zhang, J.B. Goodall, D.J. Morgan, S. Brown, R.J. Clark, J.C. Knowles, N.J. Mordan, J.R. Evans, A.F. Carley, M. Bowker, Photocatalytic activities of N-doped nano-titanias and titanium nitride, *J. Eur. Ceram. Soc.*, 29 (2009) 2343–2353.
- [30] T.N. Bahremandi, M. Fathi, A. Monshi, V. Mortazavi, F. Shirani, S.M. Mohammadi, Synthesis and evaluation of antibacterial activity of silver-doped titania nanoparticles as an antibacterial additive to dental materials, *J. New Mater.*, 4 (2013) 21–33.
- [31] M. Ahmad, E. Ahmed, W. Ahmed, A. Elhissi, Z. Hong, N. Khalid, Enhancing visible light responsive photocatalytic activity by decorating Mn-doped ZnO nanoparticles on graphene, *Ceram. Int.*, 40 (2014) 10085–10097.
- [32] D.C. Marcano, D.V. Kosynkin, J.M. Berlin, A. Sinitskii, Z. Sun, A. Slesarev, L.B. Alemany, W. Lu, J.M. Tour, Improved synthesis of graphene oxide, *ACS Nano*, 4 (2010) 4806–4814.
- [33] S. Kashyap, S. Mishra, S.K. Behera, Aqueous colloidal stability of graphene oxide and chemically converted graphene, *J. Nanopart.*, 2014 (2014) 1–6.
- [34] H.S. Shin, D. Kang, Control of size and physical properties of graphene oxide by changing the oxidation temperature, *Carbon Lett.*, 13 (2012) 39–43.
- [35] A. Derbalah, A. Ismail, Remediation technologies of diazinon and malathion residues in aquatic system, *Environ. Prot. Eng.*, 39 (2013) 135–147.
- [36] F. He, D. Zhao, J. Liu, C.B. Roberts, Stabilization of Fe- Pd nanoparticles with sodium carboxymethyl cellulose for enhanced transport and dechlorination of trichloroethylene in soil and groundwater, *Ind. Eng. Chem. Res.*, 46 (2007) 29–34.
- [37] N. Kashif, F. Ouyang, Parameters effect on heterogeneous photocatalysed degradation of phenol in aqueous dispersion of TiO₂, *J. Environ. Sci.*, 21 (2009) 527–533.
- [38] D. Mijin, M. Savić, P. Snežana, A. Smiljanić, O. Glavaški, M. Jovanović, S. Petrović, A study of the photocatalytic degradation of metatiron in ZnO water suspensions, *Desalination*, 249 (2009) 286–292.
- [39] M. Dehghani, A. Fadaei, Photocatalytic oxidation of organophosphorus pesticides using zinc oxide, *Res. J. Chem. Environ.*, 16 (2012) 104–109.
- [40] R. Mohamed, I. Mkhallid, E. Baeissa, M. Al-Rayyani, Photocatalytic degradation of methylene blue by Fe/ZnO/SiO₂ nanoparticles under visiblelight, *J. Nanotechnol.*, 2012 (2012) 1–5.
- [41] P.R. Gogate, A.B. Pandit, A review of imperative technologies for wastewater treatment I: oxidation technologies at ambient conditions, *Adv. Environ. Res.*, 8 (2004) 501–551.
- [42] M. Muneer, M. Qamar, M. Saquib, D. Bahnemann, Heterogeneous photocatalysed reaction of three selected pesticide derivatives, protham, propachlor and tebuthiuron in aqueous suspensions of titanium dioxide, *Chemosphere*, 61 (2005) 457–468.
- [43] Y. Nakaoka, H. Katsumata, S. Kaneco, T. Suzuki, K. Ohta, Photocatalytic degradation of diazinon in aqueous solution by platinumized TiO₂, *Desal. Wat. Treat.*, 13 (2010) 427–436.
- [44] N. Daneshvar, S. Aber, M.S. Dorraji, A. Khataee, M. Rasoulifard, Photocatalytic degradation of the insecticide diazinon in the presence of prepared nanocrystalline ZnO powders under irradiation of UV-C light, *Sep. Purif. Technol.*, 58 (2007) 91–98.
- [45] V. Sakkas, A. Dimou, K. Pitarakis, G. Mantis, T. Albanis, TiO₂ photocatalyzed degradation of diazinon in an aqueous medium, *Environ. Chem. Lett.*, 3 (2005) 57–61.

- [46] A.A. Khodja, T. Sehili, J.-F. Pilichowski, P. Boule, Photocatalytic degradation of 2-phenylphenol on TiO₂ and ZnO in aqueous suspensions, *J. Photochem. Photobiol. A*, 141 (2001) 231–239.
- [47] H. Hossaini, G. Moussavi, M. Farrokhi, The investigation of the LED-activated FeFNS-TiO₂ nanocatalyst for photocatalytic degradation and mineralization of organophosphate pesticides in water, *Water Res.*, 59 (2014) 130–144.
- [48] Z.-p. Yang, X.-y. Gong, C.-j. Zhang, Recyclable Fe₃O₄/hydroxyapatite composite nanoparticles for photocatalytic applications, *Chem. Eng. J.*, 165 (2010) 117–121.